Inkjet Photoresist Printing for Semiconductor Devices

Teodore Stoilevski [a], Valentyna Pawlowska [a], Lauriane Maillefort [b], Cynthia Richard [b], Catherine Marsan-Loyer [b], Sergio Ivan Yanez Sanchez [b*]
[a] University of Waterloo, Waterloo, Canada
[b] Centre de Collaboration MiQro Innovation (C2MI), Bromont, Canada.
Email: sergio.yanez@c2mi.ca

Abstract

The current industry-dominant method for photoresist deposition is spin-coating. However, as technology continues to advance, specifically in the field of microelectronic mechanical systems (MEMS), the limitations of spin-coating are becoming more apparent. A promising alternative is inkjet printing; a well-developed technology that has been very successful in a multitude of other applications, notably in 3D printing. Aside from offering good results on patterned wafers – filling cavities and eliminating edge beading – this additive technique also holds the advantage of dispensing minute volumes of photoresist, unlike spin-coating, which ejects larger volumes of resist while only 5% to 10% is retained on the substrate. Additionally, it can selectively deposit resist onto required locations on the wafer or directly print patterns, reducing the number of photolithography steps required. This article focuses on developing a process for printing photoresist for photolithography applications using a commercially available SUSS inkjet printer in a manufacturing, cleanroom environment (200 mm Fab, FED STD 209E class 10). A commercially available positive photoresist used for production within C2MI's facility – whose intended method of deposition is spin-coating – was adapted through dilutions for inkjet printing. The findings included an optimal viscosity within a range of 5.5 cPs to 7.5 cPs (with a $\pm$ 1 cPs tolerance) and a surface tension between 28 mN/m and 34 mN/m. A 4.35% coating uniformity on a 1.48 μm thick layer was achieved, on average. Furthermore, sharp printed edges without bleeding were obtained, with a print time of 62 seconds for a blanket print. A simple three-layer proof-of-concept test structure was then designed and fabricated to compare inkjet printing with traditional spin-coating photolithography. Uniformity, thickness, print time, resist volume, and the critical dimension (CD) of the photoresist coatings after photolithography were measured and compared, demonstrating promising results for inkjet printing. Although more work is still needed to bring inkjet printing from a proof-of-concept method to an industry ready technology, the control and precision offered by inkjet printing can lead to advancements in material deposition for a variety of applications in the microfabrication process of MEMS. It has the potential to overcome current limitations of spin-coating and can do so while being a more eco-responsible and cost-effective option by reducing material waste.

Key words

Inkjet printing; Additive manufacturing; Photolithography

I. Introduction

As microfabrication continues to grow towards more demanding and precise applications with multi-layered microelectromechanical systems (MEMS) devices becoming more and more common [1], photoresist deposition techniques must adapt. The traditional photoresist coating process, dating back to the 1950s from when the semiconductor industry began, has long been spin coating [2]. This method, which has dominated the industry, involves dispensing 1 mL to 5 mL of photoresist onto a spinning substrate, held on a vacuum platform and rotated at high RPM (rotations per minute) to achieve the desired thickness [3, 4]. To ensure a full and even coating of the surface, the majority of the photoresist is spun off of the substrate, making this process highly wasteful due to the excessive amounts of chemicals dispensed. For most applications – i.e., patterning a resist layer prior to metal etching – a final resist thickness varying from a few microns to nanometers is all that is required [4, 5]. Spin coating therefore results in an exceptionally low resist yield by discarding approximately 90% to 95% of the photoresist applied [3, 5, 6].

The technique evidently holds its high status in the industry due to its efficiency, repeatability, and ability to produce highly uniform coatings, which are critical for photolithography processes to output cutting-edge resolution for micro-imaging. However, many issues still arise from the process. Typically, with more viscous liquids, the edges of the substrate accumulate chemical buildup called edge beading [4], due to surface tension and the centrifugal force during the spinning process (Figure 1 (A)). Edge bead removal (EBR) is normally performed at the end of the coating process to alleviate excess resist but leads to more chemical consumption [4]. Otherwise, edge beading can lead to serious issues in applications like wafer bonding, where the elevated resist causes unevenness, leading to voids, poor adhesion, and deformation [7]. This is apparent in both blank and patterned wafers. When it comes to structured wafers however, the limitations of

spin coating become more evident. One of the most observed defects are comets (Figure 1 (B)). They occur due to large obstructions on the wafer such as solid particles like dust, or relatively higher structures and/or deep cavities on the substrate [8]. Due to the disruption of the normal radial flow, a streak forms stemming from the topographical change, creating areas where photoresist does not cover the wafer, ultimately impacting the overall functionality and quality of the end result [9].

In many cases, spin coating can lead to device-altering defects; however, in other instances it is simply not a feasible method due to the substrate's topography. For example, for muti-layered MEMS devices with high aspect ratio structures and a high loading, there is an increased chance that bubbles could form between structures, along with comets severe enough that the resist could fail to cover even half the wafer (Figure 1 (B)). In these situations, spray coating has been considered to fill the voids where spin coating reaches its limits. Spray coating can apply photoresist on top of existing structures, tackling the radial force issue associated with spin coating [10]. This method can easily coat the entirety of patterned wafers, remaining unaffected by the topography of the surface [11]. However, regardless of these potential advantages, spray coating still holds significant drawbacks. One of the most pertinent issues for MEMS applications is the uniformity of the film [12]. In a study conducted by Liming Yu *et al.*, it was reported that a layer of photoresist with a thickness of 14 μm had a uniformity of approximately 10% on the top surface and approximately 70% on the bottom surface [13]. In addition to poor uniformity, spray coating suffers from a low resist yield ranging from 5% to 15% with each coating [11]. Even if this is a slight improvement compared to spin-coating, it contributes similarly to the material waste issue. Although spray coating offers some selectivity in terms of surface area coverage which can help with material waste [12], it remains limited to larger regions of the substrate, rather than precise coverage of individual features ranging from several hundreds of microns to a few millimeters. As the nozzle diameters for spray coating range from 0.5 mm to 2.2 mm, along with a 5 mm to 15 mm spray distance and 10° to 60° spray angle, the sprayed mist covers an area of approximately 2307 mm^2, which is much larger than the average MEMS device size [14, 15]. With its large spray area, poor resolution, and excessive material consumption, spray coating presents clear limitations, making it unsuitable as a universal deposition technique, leaving a gap that needs to be bridged.

With these challenges raising questions about potential solutions, the more recently developed coating method of inkjet printing has been shown to be an alternative option to overcome issues spin and spray coating encounter. Inkjet printing – similar to 3D printing – typically utilizes Drop-on-Demand (DoD) piezoelectric actuation technology, allowing for the precise control of droplet ejection onto a substrate [16]. This mechanism enables the control of droplet size, speed, shape, and trajectory, which are all critical factors for high-quality inkjet printing [6, 17]. Unlike the other processes, this method offers precise control of the location in which micro-droplets of photoresist are dispensed on the substrate, ultimately creating the desired layout with greater efficiency and performance, as depositing resist on undesirable

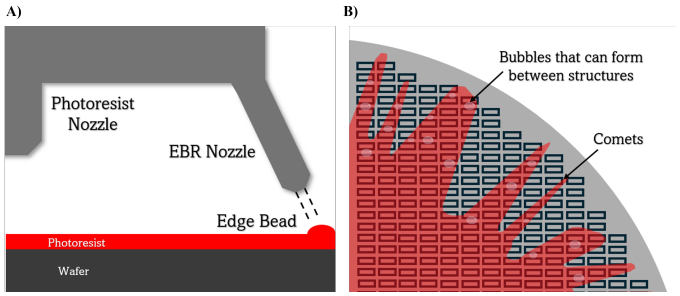

Fig. 1 Common issues that occur during the spin coating process. (A) Edge bead accumulation on the perimeter of the wafer, requiring extra solvent for removal during edge bead removal (EBR). (B) A highly structured wafer showing major defects of spin-coating such as comets and bubbles between structures.

	Spincoating	Inkjet
Uniformity	Excellent	Good (Some variation due to droplet merging + edge effects.)
Material Waste	High	Low
Step Coverage	Poor	Good
Edge beading	Significant	Negligible/None
Patterning	Indirect (Requires photomask, exposure, and development.)	Indirect/direct (Can be used with a photomask, or for maskless writing)
Resolution	Excellent	Moderate (Limited by droplet size when direct/maskless writing)
Throughput	High	Variable (Process dependent)

Table 1 Qualitative comparison of key parameters for resist spin coating and inkjet printing.

areas can contribute to a decrease in functionality. A study conducted by Chen *et al.* in 2009 found that when residual photoresist remained on the sensing material of the devices they were evaluating, it reduced the sensing performance [18]. In a similar study on layer deposition, it was found that inkjet-printed dielectric layers demonstrated higher density, fewer oxygen vacancies, and lower leakage currents compared to spin coating [19], demonstrating the potential of this method when utilized for other material and chemical coatings (see Table 1 for a comparison between spin coating and inkjet printing).

From an eco-friendly standpoint, inkjet printing maximizes the utilization of the dispensed ink, drastically reducing material waste in the photolithography process while maintaining the same functionality. This study aims to demonstrate the feasibility of inkjet printing as an alternative to spin coating for photoresist deposition in an industrial environment. We began by developing an inkjet-compatible formulation of a well-known industry

spin coated positive photoresist OiR674-11, followed by the optimization of waveform and printing parameters. Finally, after confirming photolithography characteristics, a proof-of-concept test structure was fabricated using both inkjet printing and spin coating as the photoresist deposition technique to compare process efficiency and resulting structural differences. All tests, experiments and microfabrication steps were conducted in an industrial 200 mm Fab class 10 (FED STD 209E).

II. Theory of Photoresist Formulation

To be able to print photoresists, many physical and chemical properties need to be considered to achieve optimal jetting. The solution's rheological and interfacial properties must be compatible with the printhead's specifications, while maintaining the photolithography properties of the original photoresist. Key characteristics such as surface tension, wettability, viscosity, and nozzle ejection of the photoresist play a crucial role in jetting and overall print quality. Predicting the property values of the resist dilutions was performed using literature documented properties of the utilized solvents to achieve optimal theoretical jetting and print efficiency. To predict the outcome of the surface tension a weighted average formula was used. There are more accurate methods to predicting the surface tension of a solution such as the Macleod-Sugden Equation (Parachor Method), however as the molecular weight of the commercially available OiR674-11 resist is unavailable, this method and others that are similar, could not be utilized [20]. In a similar fashion, the dynamic viscosity was predicted in way of a weighted logarithmic average. Similarly to the surface tension calculation, this approximation of viscosity was used due to a lack of available information on the resist.

The compatibility between the photoresist's characteristics and the printhead's specifications was evaluated using the dimensionless value of the Ohnesorge (Oh) number (Equation 1). As a combination of the Reynold (Re) and Weber (We) numbers, the inverse of the Ohnesorge number (Z) provides a value used to predict the droplet formation based on the nozzle diameter, factoring in surface tension, viscosity and inertial forces [21].

$$Oh = \frac{\sqrt{We}}{Re} = \frac{\eta}{\sqrt{\rho L \sigma}} = \frac{1}{Z} \tag{1}$$

Where surface tension, density, nozzle diameter, droplet velocity, and dynamic viscosity, are given by σ, ρ, L, v, and η, respectively. Ideal jetting contains a Z value that lies between $1 < Z < 10$, decreasing the risks of jetting imperfections [21]. If Z is less than 1, this signifies that the ink is too viscous, meaning there is not enough energy transferred for proper droplet ejection, if any [22]. On the contrary, if Z is greater than 10, the ink would not be viscous enough, raising risks of satellite droplets [22]. Satellite droplets lead to defects such as inconsistency and edge spitting, as they are small, uncontrolled secondary droplets that trail the main droplet.

Arguably, the most critical factor for inkjet printing of photoresists is the selection of compatible solvents. Key material properties to consider when selecting solvents, due to their impact on physical formulation performance such surface drying, nozzle ejection, solubility, and print quality—include boiling point include, but are not limited to: evaporation rate, polarity, dispersion, and hydrogen bonding [23, 24]. These are all grouped together within the solvent's Hansen Solubility Parameters (HSPs) which dictate how the photoresist interacts with the selected dilutors [24, 25]. In this study, focus was placed on the HSPs that help with inkjet related matters, more specifically the importance of selecting two solvents, one having a high boiling point and the other having a low boiling point. The purpose of a high boiler in the dilution is to reduce evaporation at the nozzle, thereby reduce nozzle clogging, and improving the jetting performance, while the low boiler aids in nozzle ejection by facilitating quick exit evaporation, leading to proper jetting and reducing the risk of clogging [26, 27].

III. Methodology

A. *Experimental Setup*

This study used a SUSS LP50 desktop inkjet printer equipped with a Konica Minolta KM512SH print head, which contains 512 nozzles, each with a 20 μm diameter. The print head is configured for a 4 pL drop volume. Prior to printing, the nozzles were primed by executing a purge of 150 mbar for 4 seconds, during which several drops are dispensed (approximately 0.09 mL total is ejected from all 512 nozzles combined), allowing for proper nozzle wetting. Maintaining wetted nozzles both before and during printing is essential for consistent resist flow, droplet formation and velocity [28]. To further ensure optimal printing conditions, nozzle wiping was performed both before and after prints as it aids with eliminating nozzle-nozzle droplet interference, which can lead to an alteration in a droplet's flight trajectory [27]. To validate this, droplet formation was observed using the LP50's Dropview camera, confirming the presence of the required droplet formation sequence.

Two wafer alignment methods are available on the LP50 inkjet printer: edge alignment and fiducial alignment. This article utilized edge wafer alignment as a sufficient and repeatable method when precise overlay is not required, as this strategy simply aligns on 5 points around the wafer. For situations where precise alignment to existing features is required (i.e. when direct droplet-to-feature inkjet printing was developed), 1 mm x 1 mm 'plus sign' fiducials were positioned at the 3 and 9 o'clock locations on the wafer as it accounts for minute changes in the wafer's orientation. For instance, a subtle angle deviation of the substrate on the chuck due to manual loading would be detected by fiducial alignment.

Following alignment, Gerber (.gbr) files were prepared and processed through the built-in SUSS Gerber Rasterizer software, which converts the vectorized layouts into the final printable format needed for the printer. The print resolution can be set in the Gerber Rasterizer, enabling the user to select high print resolution in comparison to image formats such as .png and .jpeg.

B. *Resist Characteristics*

To confirm resist-printhead compatibility, dynamic viscosity measurements were performed from 25°C to 70°C on a TA Instruments DHR-20 rheometer, equipped with a 1° cone and a 50 mm

diameter plate rotating at a constant rate of 41.89 rad/s. The viscosity of the resist formulations were measured for all dilutions using identical measurement parameters specified by the photoresist's manufacturer (FujiFilm). Preliminary experiments were conducted with all dilutions, after viscosity confirmation, to obtain results of the jetting and printing performance, as well as to confirm that the compositions could withstand C2MI's standard photolithography process for a 1 μm layer of positive photoresist. The simple tests were performed using default LP50 parameters, where preliminary experiments included a three-step process of determining if further optimization would be beneficial.

Surface tension was measured post-trials for the same purpose of printhead compatibility. The surface tension measurement was executed using pendant drop tensiometry [29].

C. Jetting and Printing Parameters

Waveform design is vital and is considered as the backbone of inkjet printing as fine-tuning the parameters correctly allows for optimal droplet speed, volume, stability, and print quality. To establish the ideal jetting conditions for any ink in the KM512SH printhead (assuming all properties of the ink are compatible with the printhead), a five-step algorithm was developped as a baseline approach. All jetting parameters were considered and are shown in Table 2. A similar parameter methodology tactic was executed through a design of experiments (DoE) to identify the optimal printing parameters. Factors such as print speed, resolution, step size, substrate temperature, and quality factor were chosen as definitive parameters that work in parallel when creating the most suitable print. Conditions for the optimal layer were based on C2MI's production standards, factoring in layer thickness, uniformity, and overall process time for 200 mm silicon wafers. Thickness and uniformity of the resist were measured by spectroscopic reflectometry using a N&K Technology tool. The resist was measured on 25 spots distributed over the wafers. Prior to selecting the final photoresist dilution, an early resist mixture was used to gain an understanding of the effects between the selected printing parameters. The print layout for all tests was a circle centered on the 200 mm wafer, with a radius of 85 mm. The executed seven-experiment DoE was based off JMP's minimum thirteen-experiment, 'Main Effects' DoE model type for five parameters. JMP is a statistical analysis software that allows simple DoE to be created by automatically generating combinations of provided values to evaluate effects between variables.

D. Photolithography Optimization

To verify whether photolithography properties deviated from those of the original, non-diluted OiR674-11 positive photoresist, a series of photolithography tests were conducted. A range of exposure doses were tested to determine the ideal dose required for proper development and adequate adhesion, subsequently resulting in conformal quality. Step exposures were executed on the Screen DW3000 maskless aligner, where the blanket layer of printed photoresist was exposed through multiple trials, with doses ranging from 130 mJ/cm^2 to 320 mJ/cm^2. These doses were selected based on standard in-house production doses for OiR674-11. The exposed mask included features ranging from 4 μm to 700 μm. To further imitate a standard production spin-coated OiR674-11 flow, HMDS – used as the adhesion promoter for the positive resist – was tested with the final dilution for adhesion enhancement and overall suitability. A development process was then optimized on the Osiris Varixx 304 developer module. The basis for the optimized development process was initially based on the production-level recipe for 1 μm of OiR674-11 in the Tokyo Electron CLEAN TRACK ACT 8 system. Tests were performed to determine an ideal developer flow rate, volume, vacuum chuck rpm, and overall development steps to cater to any layer sensitivity during development.

E. Microfabrication Process

Proof-of-concept test structures were designed and fabricated in three separate lots using inkjet-printed, as well as spin-coated, photoresists for comparison. Each lot contained three wafers to evaluate repeatability. The tests were conducted on 200 mm wafer with a 5 mm edge exclusion. The inkjet printed method was executed in two ways: a blanket layer process and a patterned (photo-trimmed) process. The purpose of a photo trimming inkjet method is to optimize photoresist consumption by limiting the coating strictly to necessary areas. The goal of the proof-of-concept was to directly compare the two coating methods in identical processes, examining differences of plasma stripping, adhesion, critical dimensions (CDs), sidewall angles, and overall quality. The fabrication consisted of a three-mask process flow, referred to as M10, M20 and M30. It is illustrated in Figure 2 (A), illustrates the photo-trimmed inkjet-printing method. The completed wafer layout and the die design is shown in Figure 2 (B). Metal and oxide etch rate tests were performed in the

Step	Parameter	Starting Value	Var.	ADA Test Range	Optimal Value
1	ON Pulse Width	2	t_1	0.5:0.5:10	2
	OFF Pulse Width	6	t_2	1:1:20	5
2	ON-to-OFF Pulse Width Delay	0	Δt	0:0.5:5	1
3	ON Pulse Voltage	16	V_H	6:1:22	18 V
	OFF Pulse Voltage	8	V_L	3:1:11	11 V
4	Drop Period	10	T_d	5:0.5:40	10
	Phase Length	20	λ	10:0.5:50	20
5	Ink Pressure	-25	P_{ink}	-35:5:-10	-25 mbar
	Firing Frequency	1	f	1:1:10	5 kHz

Table 2 Five-step waveform optimization algorithm for the KM512SH printhead. Each jetting parameter includes the default value suggested by the LP50 printer, which are typically the starting values prior to fine-tuning. Parameters were systematically varied across the inputted ranges (start:step:end) using the Advanced Dropview Analysis software to construct an optimal waveform.

SPTS Versalis FxP ICP and APS modules. As these are two types of etches done in the process flow, etch rate tests were conducted in these chambers using a 60 second recipe, measuring the thickness before and after the process. The first measured etch was for oxide which utilizes a C_4F_8, H_2 and He plasma chemistry. Subsequently, the AlCu (metal) etch rate was examined which uses an Ar and Cl_2 plasma with a BCl_3 breakthrough step. Post oxide etch, to validate that the solvent dilution didn't affect the chemical components to allow the photoresist to be stripped properly, a voltage versus time graph was extracted from the Ulvac Enviro-1Xa to analyze differences, if any.

F. *Material Waste Comparison*

To estimate the approximate volume of chemicals dispensed during inkjet printing, the following equation was considered:

$$V_{dispensed} = R_x R_y \left(\frac{A_{print}}{6.4516} \right) V_{droplet} \quad (2)$$

where R_x and R_y is the resolution (dpi) in both the x and y direction, A_{print} is the surface area of the print in cm^2, and $V_{droplet}$ is the droplet volume in mL. The surface area of the print is divided by 6.4516 to convert cm^2 to $inch^2$.

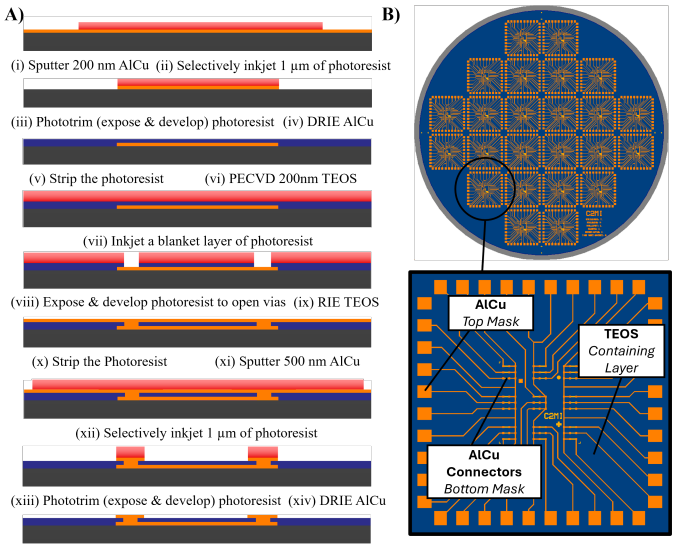

Fig. 2 Microfabrication process flow. (A) The process flow depicting the fabrication steps used to create the test structures. The structures were fabricated three times using three different photoresist deposition techniques: spin-coating, blanket inkjet-printing, and the illustrated patterned (photo-trimmed) inkjet printing. (B) Wafer and die layout of the proof-of-concept test structure.

IV. Results and Discussion

A. *Photoresist Formulation*

Numerous solvents were explored to dilute the OiR674-11 positive photoresist to an inkjet compatible form from its original viscosity and surface tensions of 15.01 mPa·s at 25°C and 25.9 mN/m, respectively. On one hand, based on early testing, the ideal viscosity was identified to be between 5.5 cPs to 7.5 cPs, with a $\pm$ 1 cPs tolerance that can be adjusted with head heating.

	Chemicals	Ratio	Theo. Purpose	Visc. (cPs)	Surface Tension (mN/m)	Theo. Visc. (cPs)	Theo. Surface Tension (mN/m)	Exp. Visc. (cPs)
1	OiR674-11	50	Photoresist	15.01	25.9	7.92	30.01	6.47
	TGME	19	High BP	7.00	31.4			
	2-Heptanone	16.5	Low BP	0.77	26.17			
	Cyrene	14.5	Raise surface tension	14.5	46.73			
2	OiR674-11	50	Photoresist	15.01	25.9	6.28	29.57	4.74
	2-Heptanone	20	Lower visc.	0.77	26.17			
	Ethyl Lactate	15	Low BP	2.44	29.2			
	Cyrene	15	High BP	14.5	46.73			
3	OiR674-11	50	Photoresist	15.01	25.9	8.49	31.48	7.20
	Cyrene	25	Raise surface tension	14.5	46.73			
	PGMEA	20	Low BP	1.1	26.4			
	TGME	5	High BP	7.00	31.4			
4	OiR674-11	50	Photoresist	15.01	25.9	5.15	33.00	4.82
	DMSO	40	High BP	1.99	43.53			
	PGMEA	10	Low BP	1.1	26.4			

Table 3 Photoresist dilutions created for testing using theoretical knowledge for estimated viscosities and surface tensions. All viscosity values listed in are at 25°C.

On the other hand, the ideal surface tension, based on preliminary testing with commercially available inkjet-compatible inks, was found to be between 28 mN/m and 34 mN/m. To avoid weak or unstable jetting, the surface tension should not fall below this range, and to avoid poor droplet detachment the surface tension should not be above this range [28]. Resists were formulated based on the previously discussed reasoning and prediction methods presented in Section I, with all theoretical values falling within the required ranges (Table 3). Most dilutions consisted of Cyrene – a bio-renewable solvent derived from cellulose and commonly used to replace harmful solvents – selected as the primary solvent in most mixtures to further align with the sustainability goals with inkjet printing. However, it had to be coupled with two solvents to lower viscosity as unlike DMSO, Cyrene has a similar viscosity to OiR674-11, making the solution too viscous for printhead compatibility.

All dilutions in Table 3 were put through a three-step analysis. The first step of the analysis consisted of observing basic droplet formation through the dropview camera, seeking full droplets and early stages of the required droplet sequence (Figure 3 (A)). The sequence – often looked at as a '1,2,3' formation (Figure 3 (B)) – is present due to the shared-wall where the same actuator is used in the nozzles (right wall of nozzle 1 has the same actuator as the left wall of nozzle 2; right wall of nozzle 2 has the same actuator as the left wall of nozzle 3). As the head is jetting, the actuator moves between its associated three nozzles, firing a droplet one nozzle at a time, giving the diagonal appearance. It is important to note that this is specific to the KM512SH printhead. From there, a print test using recommended parameter values built-in to the printer was executed through a blanket resist layer, analyzing voids and defects in the coating. Lastly, if the print trial showed a complete-enough layer, exposure and development tests were conducted to confirm that there were no severe voids or missing regions post-development. There was no evaluation of specific feature quality at this stage; it was simply to observe the layer's integrity. The chosen final dilution was 50% OiR674-11 (a product of Fuji Film), 40% Dimethyl Sulfoxide (DMSO) and 10% Propylene Glycol Monomethyl Ether Acetate (PGMEA). Using the theory presented in Section I, the results satisfy the theoretical ap-

proach when analyzing the HSPs for optimal jetting, with DMSO having a boiling point of 189°C and an evaporation rate of 0.026 (for reference n-Butyl Acetate = 1) to fit the high boiler solvent in the dilution, as well as having a viscosity and surface tension of 1.99 mPa·s at 25°C and 43.53 mN/m [30], respectively. Whereas PGMEA has a boiling point and evaporation rate of 145°C and 0.33 (nBuAc = 1) [31], respectively, to act as the low boiler solvent. In addition, PGMEA holds a viscosity of 1.1 mPa·s at 25°C according to the safety data sheet (SDS), and a surface tension of 26.4 mN/m [32]. The estimated values of the dilution were 5.15 cPs and 33.01 mN/m, fitting into the KM512SH's operational range.

With all indications pointing towards a positive outcome, the resist dilution was further optimized and characterized. The viscosity and surface tension, along with additional physical properties, were calculated and summarized in Table 4. All values fall within the printhead's ideal ranges, confirming printhead compatibility. Importantly, the dilution's Z number fell directly in the middle of the ideal $1 < Z < 10$ range (Equation 1). This validated that droplet formation should be observed.

B. *Recipe Optimization*

Once chemical and physical compatibility was confirmed, the waveform was optimized using the algorithm shown in Table 2 to reach an ideal droplet speed, volume and sequence. The algorithm intentionally tests coupled parameters in a logical order, reflecting dependencies of certain parameters on others. Prior to fine-tuning of the jetting values, default waveform parameters set on the LP50 were used as starting points to observe the droplets exiting the nozzles, regardless of the volume and speed. However, the ON pulse width was changed from its default value of 3 μs to 2 μs to be able to view the droplets in the Advanced Dropview Analysis (ADA) software. The ADA tool that is built into the LP50's user interface, functions as a combinatorial parameter sweep engine enabling smoother waveform optimization. The application allows for systematic iteration of all possible combinations based on the ranges of jetting parameters selected to view the effects on one another.

Jetting performance before and after optimization with the algorithm can be observed in Figures 3 (A) and (B), with Figure 3 (C) depicting the optimized physical waveform. The initial waveform with the starting values (Figure 3 (A)) had a droplet speed and estimated volume of 2.34 m/s and 4.63 pL on average, respectively. Focusing on speed and overall appearance of the sequence, it was far from the targeted jetting. To encompass the many possibilities of the jetting parameter combinations

Density ρ (g/cm^3)	Surface tension σ (mN/m)	Viscosity η (mPa·s) at 25°C	Contact Angle	Z
1.08	28.4	4.82	<10°	5.14

Table 4 Phisical properties and inverse Ohnesorge number (Z) for the 50% OiR674-11, 40% Dimethyl Sulfoxide (DMSO) and 10% Propylene Glycol Monomethyl Ether Acetate (PGMEA) dilution.

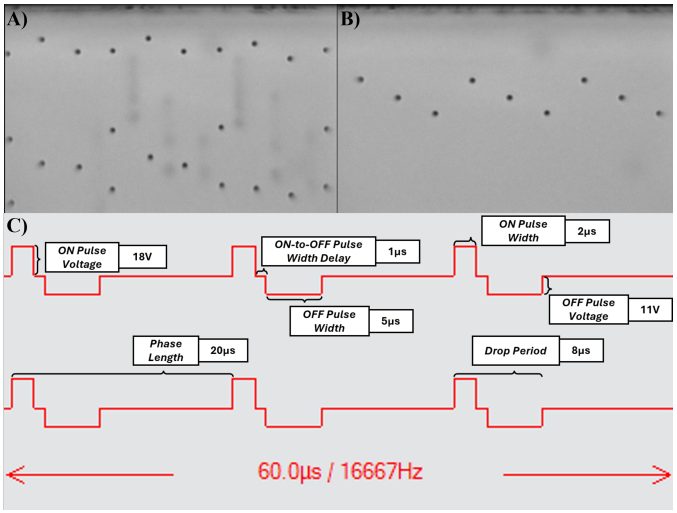

Fig. 3 Optimization of the jetting parameters for ideal droplet formation. (A) Droplet formation and instability prior to waveform optimization. (B) Droplet formation and stability after waveform optimization showcasing the desired '1,2,3' sequence. (C) The physical waveform of the final jetting parameters used for the chosen resist dilution.

a summary can be seen in the ADA Test Range column in Table 2. The series of experiments began with defining the baseline values for ON and OFF pulse widths. These parameters determine the amount of time the voltage is applied to the piezoelectric actuators, ultimately aiming to find the lowest amount of energy (minimum pulse combination) required to increase jetting efficiency and target the 6 m/s droplet speed. Following the pulse widths, Test 2 involved adjusting the ON-to-OFF pulse width, which sets a delay between the two pulses, changing the pressure in the ink chamber and enabling longer breakups between droplet exits. Once a foundation of stable, full droplets with an acceptable speed seemed to be present, Test 3 proceeded to voltage tuning. This part of the algorithm further stabilized jetting to its final form, as well as solidified droplet speed at or near the targeted 6 m/s (with secondary influence from the ink's properties). The interaction between the ON and OFF pulse voltages holds the dominant role behind the '1,2,3' droplet formation (seen in Figure 3 (B)), and ensuring a consistent speed stability between all three coupled nozzles.

Although drop period is primarily used for greyscale printing, it was included as it still represents the duration of a complete cycle in the waveform, even if it exceeds the actual total time of the ON, OFF and ON-to-OFF pulse widths combined. If required, drop period can enable a double pulse per single droplet, which has been seen to help severe satellite droplets – this was unfortunately not further explored due to complete droplets observed [33]. More significantly, phase length dictates the speed at which the actuator reaches each of it's coupled three nozzles. The ideal values would appear to have the most uniform droplet pattern, with minimal and equivalent spacing between the 3 droplets.

Post-optimization, the new values presented in the Optimal Value column in Table 2, were chosen as the ideal jetting sequence (Figure 3 (B)) which held a droplet speed and estimated volume of 5.85 m/s and 5.35 pL on average, respectively, with

some droplets having the exact speed of 6.00 m/s. Realistically, if a drop speed of approximately 6.00 m/s was reached, the droplet volume would more likely be 4 pL with a ± 10% variation. This would align with the printhead specifications and it's intended design for 4 pL droplet volume. Moreover, the waveform produced stable jetting meaning the desired '1,2,3' droplet formation held consistently, without the issue of satellite droplets forming over time, leading to consistency in prints.

One of the most important factors for developing an optimal inkjet printing recipe was to determine the CTQs (Critical to Quality Specifications) for the preferred photoresist layer. The CTQs are measurable outputs derived from the desired results, aiming to achieve a printed photoresist coating that is comparable to production-level resist layer qualities. Based on C2MI's in-house spin-coating process which takes exactly 65.8 seconds to complete, accounting for only spin coating and EBR (excluding transportation within the machine), the CTQs for the ideal printed photoresist layer and the corresponding target values are as follows: 1 μm to 2 μm layer thickness, a uniformity variation under 5%, a printing time below 2 minutes, an edge clearance ability between 1 mm and 5 mm, and no edge bleeding or excessive fluidity of the photoresist. To achieve these results, key printing parameters, shown in Table 5, were chosen and optimized utilising a DoE.

Parameter	Unit	Min	Mid	Max
Print Speed	m/s	200	300	400
Qualify Factor (QF)	-	1	5	10
Step Size	pixel	1	8	14
Resolution in X-Direction	dpi	1080.852	1441.136	1801.42
Resolution in Y-Direction	dpi	1080.852	1441.136	1801.42
Chuck Heat	°C	20	30	40

Table 5 Design of experiments (DoE) parameters used to optimize layer thickness, uniformity, print time and wafer edge clearence on the SUSS LP50.

While there are many parameters that can be added to create a more expansive DoE, these six provide immediate feedback of layer changes and throughput. The parameters are interconnected, meaning that adjusting one will often affect how others will compensate. Resolution, primarily in the x-direction due to nozzle alignment, was the first thing to consider as it directly influences the thickness of the layer. A higher resolution will dispense more droplets per inch (dpi), leading to a thicker and more uniform layer in a shorter amount of time compared to stacking multiple layers at a low dpi. Resolution values are multiples of 360.284 dpi as that aligns with the physical spacing between nozzles in the x-direction. However, increasing the droplet density also raises the risk of overflow due to surface tension and contact angle effects, leading to edge bleeding and deformation in the layout's structures. This is where chuck heat became necessary as it allows for the solvents to evaporate more quickly on the substrate, helping the print to hold the layout's intended shape.

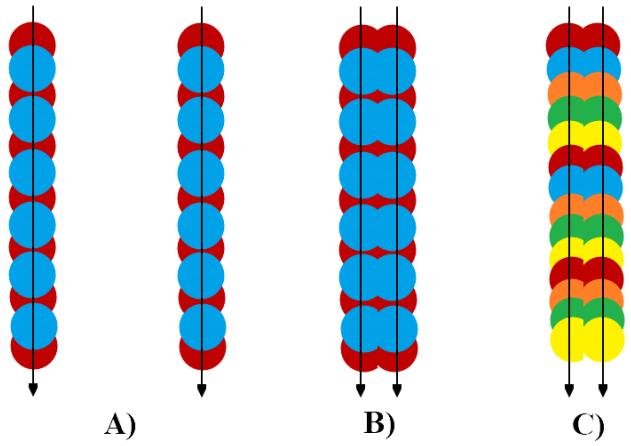

Fig. 4 Depiction of the relationship between Qualify Factor (QF) and step size. (A) Representation of a QF of 2 and a step size of 14, two nozzles (red and blue) will be used to print singular lines separated by 14 pixels. (B) A QF of 2 with a step size of 1. (C) A QF of 5 (depicted by the 5 different colors) with a step size of 1. In all cases the arrow represents the print direction.

The relationship between QF and step size dictates not only how the print will be completed, but also the number of times the printhead will pass over each swath-set (a series of print lines combined to form a 36 mm width line which is repeated across the substrate). This relationship between the two mentioned parameters directly impacts the thickness and print time. For example, in Figure 4 (A), a QF of 2 means that two nozzles (represented by blue and red) will be used to print a singular line in the scan direction represented by the arrow. This means that the printhead will pass over the wafer twice (once for each colour), completing a singular swath, prior to moving 14 pixels to print the following line. Figure 4 (B) and (C) represent a print with a QF of 2 and 5, respectively, both with a step size of 1. As illustrated, decreasing the step size to 1 creates an overlap between swath-sets, thus increasing the resolution of the print.

Originally, the set of experiments that was provided by JMP included combinations of parameters that are not permitted by the LP50 printer. More specifically, a combination such as a QF of 2, a step size of 8, with x and y resolutions of 1441.136 dpi would result in an error stating that the printhead could not complete the print as it cannot reach all areas of the layout. This occurs since the printhead's resolution is based on multiples of 360.284 dpi. When both the resolution, and the step size, are even, the alignment of the droplet placement becomes periodic and leaves repeating gaps in the printed layer. The solution is to ensure that either the resolution is an odd multiple of the base value, or that the step size is an odd number. This eliminates the symmetry issue and allows for proper pixel-to-droplet registration. Therefore, after removing and modifying some sets within the DoE based on preliminary print experiment knowledge, the final DoE consisted of seven trials. During execution, it was seen that the QF heavily influenced uniformity and print times. In addition, when comparing speeds within the original seven exper-

iments, a trend of increasing speeds and decreasing uniformity was observed, whereas the resolution was controlling the thickness and minimally influenced the print time. A final print parameter set chosen for the 50% OiR674-11, 40% DMSO, and 10% PGMEA mixture included a QF of 1, a step size of 5, a resolution of 1441.136 dpi, a substrate heat of 40°C, and a print speed of 200 m/s. This produced an evenness of 4.35% and a thickness of 1.48 μm, on average (2 wafers). A low QF combined with a relatively high resolution achieves our ideal thickness and uniformity, with a step size of 5 to offer enough overlap stitching between each 36 mm printhead swath-set (Figure 4) enabling the passes to merge seamlessly, without visible obstructions. The print took a total of 62 seconds to complete, meaning all measured values remained in the ideal CTQ ranges.

After the final recipe was selected and the layer characteristics were identified, results showed that the optimal exposure dose on silicon for the 1.48 μm thick layer was 280 mJ/cm^2 which aligned with the dose used on a 2 μm layer of the non-diluted OiR674-11. All doses under 160 mJ/cm^2 showed severe under exposure, while doses between 170 mJ/cm^2 and 240 mJ/cm^2 showed inconsistency in terms of adhesion. When the selected photoresist dilution was tested on the HMDS-treated substrate, beading and repulsion was observed (Figure 5 (A)). This likely occurred because DMSO is a highly polar solvent creating incompatibility between the adhesive coating and the printed dilution, since the mechanism behind the adhesion of HMDS is primarily governed by dispersive (non-polar) interactions rather than highly polar forces [34]. For this reason, the final exposure dose of 280 mJ/cm^2 was chosen to improve adhesion on the bare silicon surface, preventing unexposed structures smaller than 100 μm from washing out during the development process – a problem identified at lower doses (Figure 5 (B)). It was believed that slightly overexposing areas of the positive resist would increase the solubility, allowing for a less aggressive development process [35]. When development was attempted with a 2000 rpm chuck speed, all smaller features were washed away with the largest feature (a 700 μm diameter circle) having major defects (Figure 5 (C)). To overcome this recurring issue due to the absence of an adhesion promoter, a development recipe with a lower flow rate of 50 mL/min for 67 seconds and a top chuck speed of 1500 rpm was used, leading to full pattern retention, and resulted in a CD of 4 μm (Figure 5 (D)).

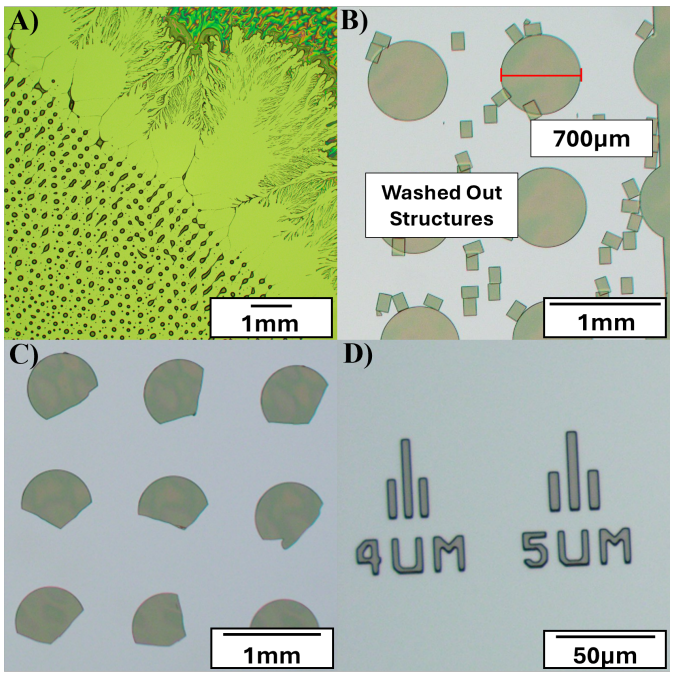

Fig. 5 Inkjet printed blanket layers using the 50% OiR674-11, 40% DMSO, and 10% PGMEA solution. (A) Image taken near the edge of the wafer depicting the incompatibility between the resist dilution and the HMDS adhesion layer. (B) An exposure test of 130 mJ/cm^2, developed using a standard recipe in the Osiris Varixx 304. (C) An exposure test of 180 mJ/cm^2, developed using a standard recipe in the CLEAN TRACK ACT 8. (D) An exposure test of 280 mJ/cm^2, developed using the optimized recipe in the Osiris Varixx 304.

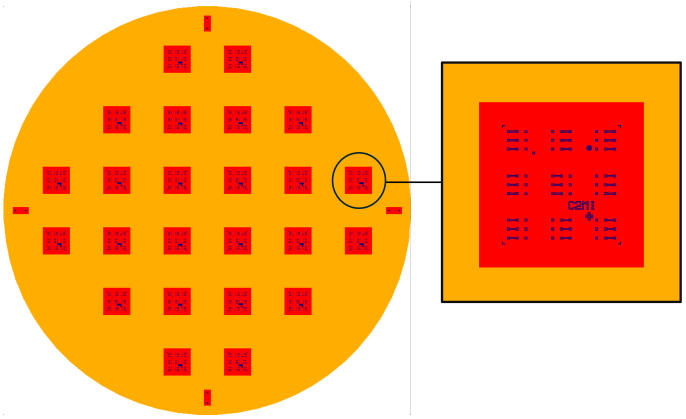

Fig. 6 First mask layout (M10). The patterned inkjet-printed resist layout is illustrated in red. It is printed over AlCu (orange). The structures in blue showcase the patterns that will remain after development.

C. *Microfabrication Process*

The final step was to further validate the compatibility of the optimized resist dilution by fabricating a proof-of-concept test structure. However, before proceeding with the fabrication process, the rate at which the photoresist layer decreases per minute during the etching step needed to be determined. The oxide etch rate for the non-diluted OiR674-11 positive resist was 160 nm/min, while the formulated solution of 50% OiR674-11, 40% DMSO and 10% PGMEA showed a slightly lower etch rate of 120 nm/min. Switching to the AlCu etch which uses an Ar and Cl_2 plasma with a BCl_3 breakthrough step, the original resist held a 175 nm/min, while surprisingly, the diluted OiR674-11 showed a big jump to 300 nm/min. The likely reasoning to these discrepancies is due to the different chemistry components that the solvents introduce.

Beginning the process of creating the test structures, an initial layer of 200 nm AlCu was deposited, followed by a photoresist coating to pattern the image of the first mask (M10) for subsequent metal etching. As expected, spin-coating exhibited an outstanding uniformity of 0.74%, with a thickness of 1.14 μm, on average. To replicate the spin-coated layer, blanket lots were printed for comparison. The values of uniformity at this desired thickness

was found to be 4.37% for the printed wafers, identical to the previously obtained results. Building on this, the inkjet-printed phototrimmed lot had three different resist layouts, one for each mask. The first mask, Mask 10 (M10) (Figure 6) which had a surface area of 1.69 cm^2 per die structure and a total surface area of 41.46 cm^2, showed an improved uniformity of 3.01% on average, with the lowest observed uniformity of 2.77% in the lot. However, it was seen that the thickness decreased from 1.41 μm to 1.17 μm, on average. The second mask, mask 20 (M20) consisted solely of a blanket printed layer for via etching, exhibited exhibited results similar to the inkjet printed lot. The photoresist coverage for the final mask, mask 30 (M30), was confined to the active dies, totaling a surface area of 222.34 cm^2 had a measured uniformity and thickness of 3.96% and 1.27 μm, respectively. By comparing the listed surface areas of each mask, a trend clearly emerged; as the surface area of the printed layout decreased, the uniformity improved, but the resist film became thinner. An explanation for this behaviour is likely due to the quick and more even solvent evaporation with smaller printed structures. Comparatively, larger printed areas require more liquid to be dispensed overall, which can result in uneven evaporation [36]. Additionally, swath overlapping and stitching – though mitigated with the printing recipe – can still attribute to variation in the film's thickness. This overlap was further reduced in the singulated patterns (Figure 6), allowing the printhead to completely pass over majority of the structures in a single motion.

A challenge arose during the exposure and development steps for M20 (TEOS vias) for the blanket-printed wafers. Post-development inspection revealed deformation on the edges of the via openings in the resist (Figure 7 (A)). Therefore, a step exposure with doses ranging from 210 mJ/cm^2 to 320 mJ/cm^2 was done on a TEOS coated wafer. The experiment indicated that 230 mJ/cm^2 was the optimal dose for the diluted resist on oxide to mitigate the issue. The defects however persisted, at a lesser degree. Upon processing the phototrimmed lot, it was expected to see similar results, but no defects were observed in the via openings on the resist layer (Figure 7 (B)). Despite an identical process on another lot, an unexpected variation was observed following photoresist development (Figures 7 (A)) potentially attributed to a faulty development step or surface contamination. Following TEOS etching, the photoresist was removed via plasma stripping. Results showed identical stripping behaviour, with both the original OiR674-11 and diluted version being fully removed after approximately 6 seconds at 5.5 V, before the plasma endpoint was detected. Figures 7 (B) and (C) depict the resist states before and after plasma stripping, showcasing no residue. The only apparent trace left behind was a coffee ring stain effect created by M10 in the phototrimmed method. As the stain was invisible to the naked eye, Figure 7 (D) is taken in the DIC mode on an optical microscope presented the ring within one of the die.

To assess the structural integrity and overall effect on the sidewall angle of the resist due to slightly overexposing it on AlCu, CD-SEM imaging was performed on M30 of both the blanket and phototrimmed inkjet methods post-development. As expected, when the spin-coated lot was analyzed, it clearly showed a perfect 90°angle, and similarly, so did both the lots of the inkjet-printed solutions (Figure 8 (A)). This confirmed that despite the un-ordinary chosen exposure dose for adhesion purposes, it had no negative effect on the resist's profile. Another SEM imagery was conducted through cross-sectional inspection after all the wafer lots were completed. The anticipated results would hopefully show all three layers: 200 nm AlCu 1st layer, 400 nm TEOS, 500 nm AlCu 2nd layer, and the 700 nm AlCu via. Upon dissection, all cross-sections noticeably showed the defined layers, with a small variation of the oxide layer being approximately 60 nm thinner than presumed. Figure 8 (B) shows the cross-section of a spin-coat processed wafer, showing an oxide etch angle of 79.61°. Almost identical results were observed for both the blanket (Figure 8 (C)) and phototrimmed (Figure 8 (D)) inkjet methods, but there was a minor variation in the oxide etched angle at 73.12° and 74.02°, respectively. This is likely caused by a difference in photoresist erosion during the etch.

A final comparison was made between the two coating methods on dispensed volumes. One spin-coated wafer resulted in 1.5 mL of resist dispensed, along with approximately 5 mL of EBR used. EBR is dispensed over a period of 9 seconds in the process and as the flow rate is not stated on the CLEAN TRACK ACT 8, a generous estimation of 5 mL was made, but can easily attain 7 mL to 10 mL of solvent used depending on flow rate. Therefore, with three layers of photoresist deposited to fabricate our test structures, a total of 19.5 mL of chemicals was used per wafer –

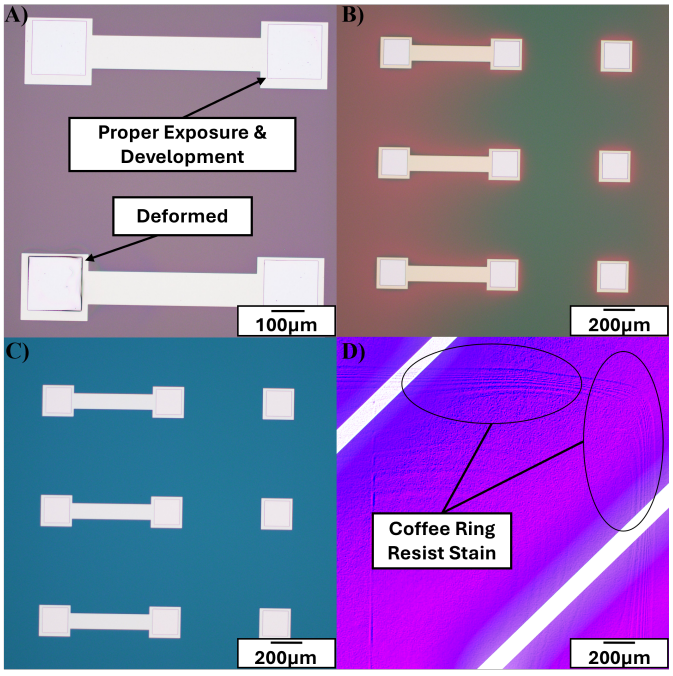

Fig. 7 Photolithography tests performed on 50% OiR674-11, 40% DMSO, and 10% PGMEA solution layers. (A) Exposure dose of 280 mJ/cm^2 demonstrating the differences between the properly exposed vias and ones with deformed edges for M20 (printed blanket layer). (B) Image taken after TEOS RIE (reactive ion etch), using a 230 mJ/cm^2 exposed photoresist layer for M20 of the phototrimmed process. (C) Image taken after photoresist stripping for the phototrimmed process. (D) Image taken in DIC mode (with post image processing) showing the coffee ring stain on the printed M10 phototrimmed process.

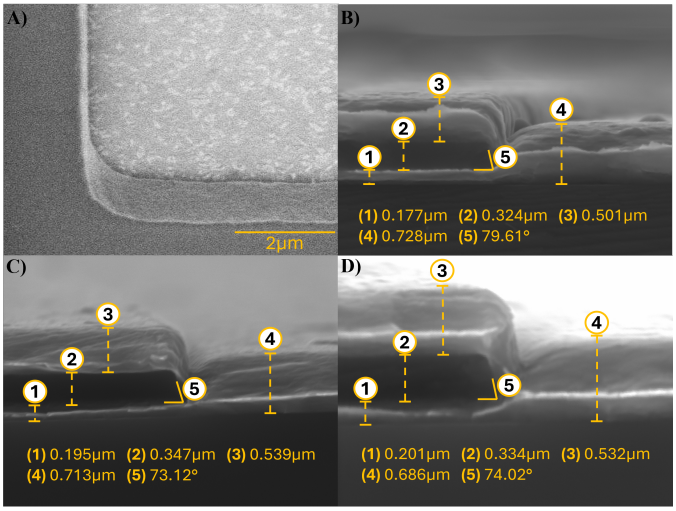

Fig. 8 Comparison of test structure formation following the microfabrication process with the 50% OiR674-11, 40% DMSO, and 10% PGMEA resist solution. (A) CD-SEM image at a 40° tilt to assess the sidewall angle post exposure with a dose of 230 mJ/cm^2 (M20). (B) cross-sectional SEM image of the spin-coated method. (C) cross-sectional SEM image of the blanket printed method. (D) cross-sectional SEM image of the phototrimmed inkjet method.

4.5 mL of photoresist and an estimated 15 mL of PGMEA (EBR). In contrast, by weighing the wafer before and after photoresist deposition via inkjet-printing, it was shown that a single blanket layer with a 5 mm edge clearance only used 0.19 mL on average. Now, this doesn't compensate for solvent evaporation, but given a droplet volume of 5.35 pL, an x-y resolution of 1441.136 dpi and a blanket surface area of 283.53 cm^2, we obtain from Equation 2 a theoretical volume of 0.488 mL for each layer. Thus, the total volume for the three blanket layers is 1.46 mL, which coresponds to 0.73 mL of OiR 674-11, 0.584 of DMSO and 0.146 of PGMEA. This is approximately a 13x decrease in material use from the spin coat method. Even further, when measuring the weight of the wafers processed with the phototrimmed method, the total amount of chemicals used was 0.348 mL (0.0146 mL for M10, 0.19 mL for M20, and 0.143 mL for M30). As discussed, since M10 has a predominantly smaller surface area compared to M20 and M30, this weighed lighter due to quicker solvent evaporation. Again, if the theoretical dispensed volume (0.0713 mL, 0.4877 mL, and 0.3823 mL for M10, M20, and M30, respectively, see Equation 2) was considered, the total volume of 0.9413 mL would output an outstanding materials savings of an approximate 21x decrease from spin-coating.

V. Conclusions

Inkjet printing is a promising technique for the deposition of photoresists, offering versatility and controlled layer-by-layer printing. With the capabilities of precise droplet placement, reduced material consumption, and control over layer characteristics, this method overcomes the limitation of traditional methods such as spin coating or spray coating. In this study, after creating the dilution of the OiR674-11 using a 50:40:10 ratio with DMSO and PGMEA, respectively, an optimized waveform (V_H = 18 V, V_L = 1 V, t_1 = 2 μs, t_2 = 5 μs, Δt = 1 μs, λ = 20 μs, f = 5 kHz) was created with a systematic five-step algorithm. Based on the target layer characteristics established from the in-house C2MI spin-coated standards a printing recipe was developed, achieving a 1.48 μm thick layer with a 4.35% uniformity, and a total printing time of 62 seconds on 200 mm wafers. It was found that the ideal exposure dose for the new resist was generally 280 mJ/cm^2, with the findings of a dose exception of 230 mJ/cm^2 on oxide surfaces. To test the photolithography of the inkjet printed photoresist versus the spin-coated, non-diluted OiR674-11 positive resist, a three-layer process was completed at C2MI's facility (200 mm industrial Fab, FED STD 209E class 10). Results showed almost identical layer thicknesses and quality, with the observation that the diluted resist may erode slightly quicker due to the etch angle of the TEOS. However, as demonstrated, it is comparable to spin coating for a simple device with the added advantage of substantial material savings, reaching up to 21 times less material used. Inkjet printing aspires to further optimize workflow by removing intermediate steps such as exposure and development, allowing for the direct coating of the desired pattern on the substrate. While this work was performed using a desktop-scale research printer, the process is readily scalable for high-volume manufacturing (HVM). Production-grade tool designed for high throughput and industrial reliability are available on the market [37, 38]. As research continues and more studies emerge, inkjet printing is becoming a compelling technique for a variety of applications and has the potential to be used as an industry-wide photoresist coating method for future technologies.

Acknowledgements

The authors would like to thank Anthony Hangoc from University of Waterloo, Benjamin Busseniers from IBM Bromont and Vincent St-Onge from the University of Sherbrooke for their help and support in the photoresist property characterizations. We further acknowledge the technical support of SUSS for collaborative development on their LP50 tool. Finally, we acknowledge the financial support from MEIE (Quebec, Canada).

References

1 K. Machida, D. Yamane, T. Konishi, S. ichi Iida, N. Ishihara, T.-F. M. Chang, M. Sone, H. Ito, and K. Masu, "Mems accelerometer fabricated by gold multi-layer metal technology," *ECS Transactions*, vol. 92, pp. 169–184, 7 2019.

2 P. Liu, L. Huang, C. Zheng, Y. Bao, D. Gao, and G. Zhou, "Spin coating in semiconductor lithography: Advances in modeling and future prospects," *Microelectronic Engineering*, vol. 298, p. 112326, 2025.

3 M. I. Hossain and S. Mansour, "A critical overview of thin films coating technologies for energy applications," *Cogent Engineering*, vol. 10, 2023.

4 J. Griffin, E. Spooner, and H. Hassan, "Spin coating: Complete guide to theory and techniques." `https://www.ossila.com/pages/spin-coating#spin-coating-general-theory`, 2024.

5 N. Sahu and S. Panigrahi, "Fundamental understanding and modeling of spin coating process : A review," tech. rep., 2009.

6 X. Wang, F. Yang, G. Guo, J. Li, Y. Sun, and L. Zhang, "Inkjet

printing photoresist with ultralow viscosity on silicon wafers for uniform coating," *Langmuir*, vol. 40, pp. 11125–11133, 5 2024.

7 S. Tuomikoski and S. Franssila, "Wafer-level bonding of mems structures with su-8 epoxy photoresist," tech. rep., 2004.

8 M. Tyona, "A theoritical study on spin coating technique," *Advances in materials Research*, vol. 2, pp. 195–208, 12 2013.

9 "Common defects found with spin coating," *Coating Systems, INc*.

10 N. Atthi, K. Saejok, J. Supadech, W. Jeamsaksiri, O. Thongsuk, P. Dulyaseree, C. Hruanun, and A. Poyai, "Improvement of photoresist film coverage on high topology surface with spray coating technique," tech. rep., 2010.

11 M. Arnold, A. Voigt, S. Haas, F. Schwenzer, G. Schwenzer, D. Reuter, G. Gruetzner, and T. Geßner, "Spray-coatable negative photoresist for high topography mems applications," *Journal of Micromechanics and Microengineering*, vol. 27, 2017.

12 N. P. Pham, J. N. Burghartz, and P. M. Sarro, "Spray coating of photoresist for pattern transfer on high topography surfaces," *Journal of Micromechanics and Microengineering*, vol. 15, pp. 691–697, 4 2005.

13 L. Yu, Y. Y. Lee, F. E. Tay, and C. Iliescu, "Spray coating of photoresist for 3d microstructures with different geometries," *Journal of Physics: Conference Series*, vol. 34, pp. 937–942, 4 2006.

14 M. A. Betz, P. Büchele, M. Brünnler, S. Deml, and A. Lechner, "Silicon micro venturi nozzles for cost-efficient spray coating of thin organic p3ht/pcbm layers," *Journal of Micromechanics and Microengineering*, vol. 27, 2017.

15 N. Koračin, M. Zupančič, F. Vrečer, G. Hudovornik, and I. Golobič, "Characterization of the spray droplets and spray pattern by means of innovative optical microscopy measurement method with the high-speed camera," *International Journal of Pharmaceutics*, vol. 629, 12 2022.

16 P. O'shea, "Driving piezoelectric actuators in industrial inkjet printers," *Power Electronics News*, 2016.

17 Z. Yang, H. Tian, C. Wang, X. Li, X. Chen, X. Chen, and J. Shao, "Piezoelectric drop-on-demand inkjet printing with ultra-high droplet velocity," *Research*, 10 2023.

18 L. T. Chen, J. S. Chang, C. Y. Hsu, and W. H. Cheng, "Fabrication and performance of mems-based pressure sensor packages using patterned ultra-thick photoresists," *Sensors*, vol. 9, pp. 6200–6218, 6 2009.

19 W. Cai, H. Ning, Z. Zhu, J. Wei, S. Zhou, R. Yao, Z. Fang, X. Huang, X. Lu, and J. Peng, "Investigation of direct inkjet-printed versus spin-coated zro2 for sputter igzo thin film transistor," *Nanoscale Research Letters*, vol. 14, 2019.

20 T. Fechter, R. Villablanca, V. Leontijevic, A. Martin, P. Jaeger, and M. J. Cocero, "Interfacial tension of water near to critical conditions by using the pendant drop method: New experimental data and a correlation based on the parachor method," *Journal of Supercritical Fluids*, vol. 196, 5 2023.

21 A. A. Castrejón-Pita, E. S. Betton, N. Campbell, N. Jackson, J. Morgan, T. R. Tuladhar, D. C. Vadillo, and . J. R. Castrejón-Pita, "Formulation, quality, cleaning and other advances in inkjet printing," tech. rep., 2020.

22 F. Iervolino, R. Suriano, M. Scolari, I. Gelmi, L. Castoldi, and M. Levi, "Inkjet printing of a benzocyclobutene-based polymer as a low-k material for electronic applications," *ACS Omega*, vol. 6, pp. 15892–15902, 6 2021.

23 D. Cvetković, M. M. Dankulov, A. Bogojević, S. Lazović, and D. Obradović, "Enhancing hansen solubility predictions with molecular and graph-based approaches," *Chemometrics and Intelligent Laboratory Systems*, vol. 251, 8 2024.

24 C. Gao, Y. Zhang, S. Mia, T. Xing, and G. Chen, "Development of inkjet printing ink based on component solubility parameters and its properties," *Colloids and Surfaces A: Physicochemical and Engineering Aspects*, vol. 609, 1 2021.

25 D. Mathieu, "Pencil and paper estimation of hansen solubility parameters," *ACS Omega*, vol. 3, pp. 17049–17056, 12 2018.

26 Q. Zhao, T. Morawietz, P. Gazdzicki, and K. A. Friedrich, "Effect of high-boiling point solvents on inkjet printing of catalyst layers for proton exchange membrane fuel cells," *Electrochimica Acta*, vol. 508, p. 145273, 2024.

27 H. Jiang, R. Qian, T. Yang, Y. Guo, D. Yuan, B. Tang, R. Zhou, H. Li, and G. Zhou, "Inkjet-printed dielectric layer for the enhancement of electrowetting display devices," *Nanomaterials*, vol. 14, 2 2024.

28 B. He, S. Yang, Z. Qin, B. Wen, and C. Zhang, "The roles of wettability and surface tension in droplet formation during inkjet printing," *Scientific Reports*, vol. 7, 12 2017.

29 J. D. Berry, M. J. Neeson, R. R. Dagastine, D. Y. Chan, and R. F. Tabor, "Measurement of surface and interfacial tension using pendant drop tensiometry," 9 2015.

30 G. Chemical, "Introduction to dmso physical properties."

31 M. Chemical, "Propylene glycol mono methyl ether acetate (pmac)," *Technical Product Information*, 2021.

32 D. C. Co, "The glycol ethers handbook," *Midland, MI: Dow Chemical Co pp 97*, 1990.

33 J. C. Arango, C. J. Pintro, A. Singh, and S. A. Claridge, "Inkjet printing of nanoscale functional patterns on 2d crystalline materials and transfer to soft materials," *ACS Applied Materials and Interfaces*, vol. 16, pp. 8055–8065, 2 2024.

34 C. Reichardt and T. Welton, *Solvents and Solvent Effects in Organic Chemistry*. Wiley, 10 2010.

35 A. Ayodele, "Positive vs. negative photoresist: A comprehensive guide to photolithography in semiconductor fabrication," *Wevolver*, 10 2024.

36 N. Tu, J. C. Lo, and S. W. Lee, "Development of uniform polydimethylsiloxane arrays through inkjet printing," *Polymers*, vol. 15, 1 2023.

37 SUSS, "JETx: Inkjet Printing Solution for High Volume Production." `https://www.suss.com/en/products-solutions/inkjet-printing/jetx`, 2025.

38 N. Systems, "Inkjet Solutions for the Semiconductor Industry." `https://www.notion-systems.com/products/Industrial-solutions/semiconductor.html`, 2025.